

Exact solutions of a time-fractional modified KdV equation via bifurcation analysis

Min-Yuan Liu(刘敏远), Hui Xu(许慧), and Zeng-Gui Wang(王增桂)
Citation: Chin. Phys. B, 2023, 32 (**12**): 120204. DOI: 10.1088/1674-1056/acf9e8
Journal homepage: http://cpb.iphy.ac.cn; http://iopscience.iop.org/cpb

What follows is a list of articles you may be interested in

A nonlocal Boussinesq equation: Multiple-soliton solutions and symmetry analysis

Xi-zhong Liu(刘希忠) and Jun Yu(俞军)
Chin. Phys. B, 2022, 31 (**5**): 050201. DOI: 10.1088/1674-1056/ac43a7

Anti-function solution of uniaxial anisotropic Stoner-Wohlfarth model

Kun Zheng(郑坤), Yu Miao(缪宇), Tong Li(李通), Shuang-Long Yang(杨双龙), Li Xi(席力), Yang Yang(杨洋), Dun Zhao(赵敦), and De-Sheng Xue(薛德胜)
Chin. Phys. B, 2022, 31 (**4**): 040202. DOI: 10.1088/1674-1056/ac401e

Multiple solutions and hysteresis in the flows driven by surface with antisymmetric velocity profile

Xiao-Feng Shi(石晓峰), Dong-Jun Ma(马东军), Zong-Qiang Ma(马宗强), De-Jun Sun(孙德军), and Pei Wang(王裴)
Chin. Phys. B, 2021, 30 (**9**): 090201. DOI: 10.1088/1674-1056/abf7a6

Bifurcation analysis and exact traveling wave solutions for (2+1)-dimensional generalized modified dispersive water wave equation

Ming Song(宋明)†, Beidan Wang(王贝丹), and Jun Cao(曹军)
Chin. Phys. B, 2020, 29 (**10**): 100206. DOI: 10.1088/1674-1056/ab9f27

Stability and Neimark-Sacker bifurcation analysis of food-limited population model with time delay

Jiang Xiao-Wei (姜晓伟), Guan Zhi-Hong (关治洪), Zhang Xian-He (张先鹤), Zhang Ding-Xue (张顶学), Liu Feng (刘峰)
Chin. Phys. B, 2013, 22 (**3**): 030204. DOI: 10.1088/1674-1056/22/3/030204

Exact solutions of a time-fractional modified KdV equation via bifurcation analysis

Min-Yuan Liu(刘敏远), Hui Xu(许慧), and Zeng-Gui Wang(王增桂)[†]

School of Mathematical Sciences, Liaocheng University, Liaocheng 252059, *China*

(Received 7 August 2023; revised manuscript received 14 September 2023; accepted manuscript online 15 September 2023)

The time-fractional modified Korteweg–de Vries (KdV) equation is committed to establish exact solutions by employing the bifurcation method. Firstly, the phase portraits and related qualitative analysis are comprehensively provided. Then, we give parametric expressions of different types of solutions matching with the corresponding orbits. Finally, solution profiles, 3D and density plots of some solutions are presented with proper parametric choices.

Keywords: the time-fractional modified KdV equation, bifurcation analysis, exact solutions

PACS: 02.30.Oz, 02.30.Jr, 04.20.Jb **DOI:** 10.1088/1674-1056/acf9e8

1. Introduction

Fractional-order partial differential equations are prevalently employed to model numerous complex phenomena involving viscoelasticity, electromagnetism, materials science, electrical networks, and fluid dynamics, etc., and interpreted best in inhomogeneous media particularly. The exact solutions of nonlinear evolution equations, which aid us in perusing the hidden physical properties, have been continuously constructed. So far, a multitude of effective methods of solving for exact solutions, including Hirota bilinear transformation,[1,2] homotopy perturbation method,[3] bifurcation method,[4–6] Darboux transformation,[7–9] generalized Kudryashov method,[10–12] inverse scattering method,[13,14] Lie symmetry analysis,[15] and so on, have been popularly adopted.

Recently, Ma[16–19] have provided some new wave equations, including integrable nonlinear Schrödinger type equations, AKNS type integrable equation and modified Korteweg–de Vries (KdV) type integrable equations. In this paper, we investigate a time-fractional order modified KdV equation[20]

$$D_t^{\alpha}u + au^2u_x + bu_{xxx} = 0,\ \ t > 0,\ \ 0 < \alpha \le 1, \tag{1}$$

where a and b are arbitrary constants. Equation (1) is well known in the explanation of physical science phenomena such as particle vibrations in lattices, thermodynamics and current flow.

Until now, (G'/G)-expansion method and improved (G'/G)-expansion method were adopted by Sahoo and Ray[20] to find soliton solutions, and the $\exp_a$ function method was carried out to Eq. (1) by Zafar.[21] Based on shifted Jacobi polynomials, Bhrawy *et al.*[22] calculated high accurate approximate solutions via a numerical method. Numerical solutions were generated via using the modified homotopy analysis Laplace transform method by Li *et al.*,[23] and semi-analytical solutions were yielded with a new variational method.[24] Alternatively, Akbulut and Kaplan[25] utilized auxiliary equation method to seek exact solutions successfully. Wang and Xu[26] provided Lie group analysis of Eq. (1) and constructed ecplicit solutions through symmetry reduction.

Bifurcation analysis[27–30] is a geometrically intuitive method to present exact traveling wave solutions. Under bifurcation theory, the types of orbits are highly tied to the sorts of solutions, which benefits us to classify solutions theoretically. Generally, the existence of periodic and homoclinic orbits signifies that Eq. (1) exists periodic and soliton solutions, correspondingly. Further, kink (or anti-kink), breaking wave solutions are separately attached to open and heteroclinic orbits. Moreover, supposing that $u(\vartheta)$ $(\vartheta = \vartheta(x,t))$ is a continuous solution of Eq. (1) and satisfying $\lim\limits_{\vartheta\to\pm\infty} u(\vartheta) = n_{\pm}$, we can say that u is a soliton solution for $n_+ = n_-$. Otherwise, u is a kink (or anti-kink) solution. As far as we know, Liang and Tang[31] only performed bifurcation analysis when integration constant is zero. Here, we consider a more general case, i.e., we provide related discussion when the integration constant is an arbitrary constant.

Let G: $[0,\infty] \to R$, the conformable fractional derivative of order β[32] is defined as

$$D_t^{\beta}(G)(t) = \lim_{\delta\to 0}\frac{G(t+\delta t^{1-\beta}) - G(t)}{\delta},\ \ t > 0.$$

The following properties are satisfied:

$$\begin{aligned}
&D_t^{\beta}(cG \pm dH) = cD_t^{\beta}(G) \pm dD_t^{\beta}(H),\ \ c,d \in R,\\
&D_t^{\beta}(t^{\lambda}) = \lambda t^{\lambda-\beta},\ \lambda \in R,\\
&D_t^{\beta}(GH) = GD_t^{\beta}(H) + HD_t^{\beta}(G),\\
&D_t^{\beta}\left(\frac{G}{H}\right) = \frac{GD_t^{\beta}(H) - HD_t^{\beta}(G)}{H^2}.
\end{aligned}$$

[†]Corresponding author. E-mail: wangzenggui@lcu.edu.cn

© 2023 Chinese Physical Society and IOP Publishing Ltd

The continuation plots are designed as follows: In Section 2, we analyze the phase portraits of the time-fractional modified KdV equation. Based on different orbits of the phase portraits, three types of new exact solutions are obtained in Section 3. In Section 4, we graphically illustrate some solutions via presenting solution profiles, 3D and density plots. Section 5 gives a summary.

2. Phase portraits and bifurcation

Equation (1) is executed to perform traveling wave transformation

$$u=\varphi(\eta),\quad \eta=kx-vt^{\alpha}, \tag{2}$$

where k and v are arbitrary parameters. Hence, Eq. (1) is turned into an integer-order ODE

$$-\alpha v\varphi'+ak\varphi^2\varphi'+bk^3\varphi'''=0. \tag{3}$$

Subsequently, integrating once over η and fixing integration constant to be c, we readily access

$$-\alpha v\varphi+\frac{ak}{3}\varphi^3+bk^3\varphi''=c. \tag{4}$$

In turn, Eq. (4) can be equivalently represented as a planar dynamical system

$$\begin{aligned}\frac{\mathrm{d}\varphi}{\mathrm{d}\eta}&=\vartheta,\\ \frac{\mathrm{d}\vartheta}{\mathrm{d}\eta}&=M\varphi^3-N\varphi+D,\end{aligned} \tag{5}$$

where $M=-\dfrac{a}{3bk^2}$, $N=-\dfrac{\alpha v}{bk^3}$, and $D=\dfrac{c}{bk^3}$.

System (5) is called a Hamilton system for $\varphi'=\partial H/\partial\vartheta$, $\vartheta'=-\partial H/\partial\varphi$, where H is defined as a Hamiltonian function

$$H(\varphi,\vartheta)=\frac{1}{2}\vartheta^2-\frac{1}{4}M\varphi^4+\frac{1}{2}N\varphi^2-D\varphi. \tag{6}$$

Further, system (5) is also conservative due to $\frac{\partial\varphi'}{\partial\varphi}+\frac{\partial\vartheta'}{\partial\vartheta}=0$. $H(\varphi,\vartheta)$ is a conserved quantity since it is not dependent on η. Therefore, H is written as

$$\frac{1}{2}\vartheta^2-\frac{1}{4}M\varphi^4+\frac{1}{2}N\varphi^2-D\varphi=\rho, \tag{7}$$

where ρ is a parameter.

Let us suppose

$$\varpi(\varphi)=M\varphi^3-N\varphi. \tag{8}$$

When $\varpi=0$, three zero roots of ϖ are identified as follows:

$$\varphi_1=-\sqrt{\frac{N}{M}},\quad \varphi_2=0,\quad \varphi_3=\sqrt{\frac{N}{M}}. \tag{9}$$

Two extreme value points of ϖ read

$$\tilde{\varphi}_1=-\sqrt{\frac{N}{3M}},\quad \tilde{\varphi}_3=\sqrt{\frac{N}{3M}}, \tag{10}$$

and the extreme values are given by

$$\begin{aligned}D_0&=|\varpi(\tilde{\varphi}_1)|=\frac{2|N|}{3}\sqrt{\frac{N}{3M}},\\ -D_0&=|\varpi(\tilde{\varphi}_3)|=-\frac{2|N|}{3}\sqrt{\frac{N}{3M}}.\end{aligned} \tag{11}$$

If assume the equilibrium points of system (5) are $(\varphi_i,0)$, the values of ρ will be

$$\rho_i=H(\varphi_i,0),\quad (i=1,\ 2,\ 3).$$

Via qualitative theory[4] of differential equations, we know that $(\varphi_i,0)$ is a center point when $\varpi'(\varphi_i)<0$; when $\varpi'(\varphi_i)>0$, $(\varphi_i,0)$ is defined as a saddle point; $(\varphi_i,0)$ becomes a degraded saddle point when $\varpi'(\varphi)=0$.

2.1. Analysis for $M>0$ and $N>0$

The phase portraits of system (5) are graphically summarized for $M>0$, $N>0$. Depending on the values of D, we present seven situations: (a) $D<-D_0$, (b) $D=-D_0$, (c) $-D_0<D<0$, (d) $D=0$, (e) $0<D<D_0$, (f) $D=D_0$, (g) $D>D_0$ in Fig. 1.

Here, we make the situations of Figs. 1(d), 1(e), and 1(f) as examples and discuss them in detail. The classification of equilibrium points is established through qualitative theory, as listed in Table 1.

Table 1. Classification of equilibrium points with different values of D.

Value of D	A	B	C
$D=0$	center point	saddle point	saddle point
$0<D<D_0$	center point	saddle point	saddle point
$D=D_0$	saddle point	degraded saddle point	degraded saddle point

Based on Fig. 1 and Table 1, the conclusions about the relationship between ρ and the types of orbits are exhibited.

Conclusion 1 When $D=0$, see Fig. 1(d).

(1) For $\rho\le\rho_2$, system (5) remains bounded open orbits with hyperbolic shape in black and pink, which states that Eq. (1) has breaking wave solutions.

(2) For $\rho_2<\rho<\rho_1$, a periodic orbit enveloping the center point A and matching a periodic solution is outlined visually. There exist two bounded open orbits in blue which are relevant to breaking wave solutions.

(3) For $\rho=\rho_1$, there are two heteroclinic orbits running through saddle points B, C and two special orbits in red, which

refers that kink (or anti-kink), singular solutions are yielded, individually.

(4) For $\rho > \rho_1$, no closed orbit is produced.

Conclusion 2 When $0 < D < D_0$, see Fig. 1(e).

(1) For $\rho \leq \rho_2$, bounded open orbits in gold and black associated with breaking wave solutions are pointed out.

(2) For $\rho_2 < \rho < \rho_3$, Eq. (1) contains periodic, breaking wave solutions which correspond to periodic, open orbits in pink, respectively.

(3) For $\rho = \rho_3$, homoclinic orbit in red going through saddle point B is described, which indicates there lies soliton solution. In addition, open and special orbits are revealed.

(4) For $\rho > \rho_3$, there is no closed orbit.

Conclusion 3 When $D = D_0$, see Fig. 1(f).

(1) For $\rho = \rho_2$, two special orbits in red are shown, which demonstrates that Eq. (1) produces singular solutions.

(2) For $\rho < \rho_2$, system (5) yields two open orbits in green matching with breaking wave solutions.

(3) For $\rho_2 < \rho < \rho_1$, there exist two open orbits in yellow.

(4) For $\rho \geq \rho_1$, no closed orbit is obtained.

2.2. Analysis for $M < 0$ and $N < 0$

For $M < 0$, $N < 0$, we draw the following phase portraits in Fig. 2. Analogously, we classify the equilibrium points that are arranged in Table 2. According to Fig. 2 and Table 2, we illustrate the following conclusions.

Conclusion 4 When $D = 0$, see Fig. 2(d).

(1) For $\rho = \rho_2$, system (5) contains two homoclinic orbits in black passing through saddle point A, referring that soliton solutions are owned.

(2) For $\rho_1 < \rho < \rho_2$, two periodic orbits in pink encircling center points B, C are drawn, so Eq. (1) has periodic solutions.

(3) For $\rho > \rho_2$, there exists a periodic orbit in blue laying outside the homoclinic orbits.

(4) For $\rho \leq \rho_1$, no closed orbit is pointed out.

Conclusion 5 When $0 < D < D_0$, see Fig. 2(e).

(1) For $\rho = \rho_2$, two homoclinic orbits in red meet at saddle point A, from which we perceive that Eq. (1) has soliton solutions.

(2) For $\rho_1 < \rho < \rho_2$, system (5) reveals periodic orbits in pink matching periodic solutions and surrounding the center points B, C, separately.

(3) For $\rho_3 < \rho \leq \rho_1$, periodic orbits in green and in yellow are shown.

(4) For $\rho > \rho_2$, a periodic orbit in blue lies outside the homoclinic orbits.

(5) For $\rho \leq \rho_3$, there is no closed orbit.

Conclusion 6 When $D = D_0$, see Fig. 2(f).

(1) For $\rho = \rho_1$, a homoclinic orbit in red is plotted, which implies that Eq. (1) has soliton solution.

(2) For $\rho_3 < \rho < \rho_1$, a periodic orbit corresponding to periodic solution in blue is yielded.

(3) For $\rho > \rho_1$, a periodic orbit in green is displayed outside.

(4) For $\rho \leq \rho_3$, no closed orbit is obtained.

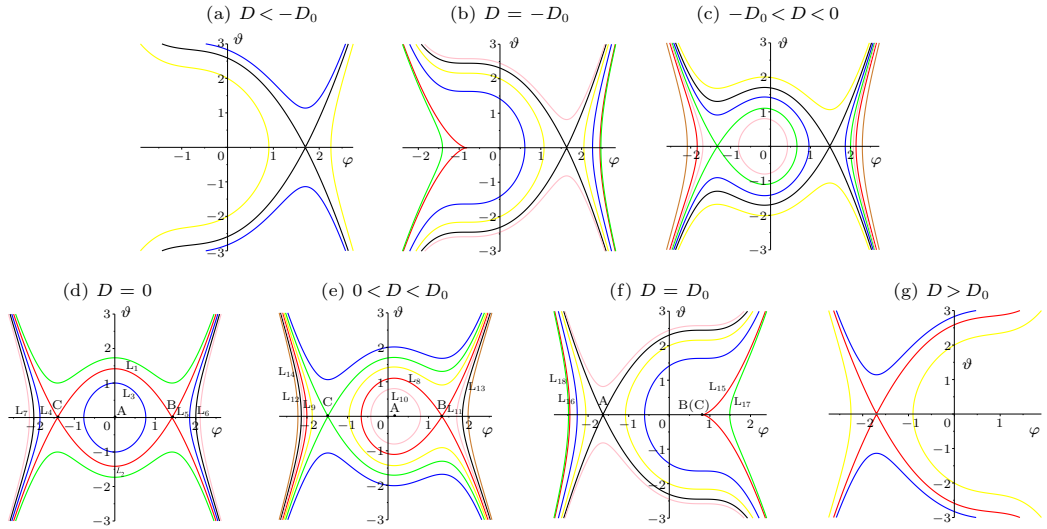


Fig. 1. Phase portraits of system (5) with $b = -1$, $k = 1$, $a = 3$, $\alpha = \frac{1}{2}$, $v = 4$: (a) $c = 1.5$, (b) $c = \frac{4}{3}\sqrt{\frac{2}{3}}$, (c) $c = 0.3$, (d) $c = 0$, (e) $c = -0.3$, (f) $c = -\frac{4}{3}\sqrt{\frac{2}{3}}$, (g) $c = -1.5$.

Table 2. Classification of equilibrium points with different values of D.

Value of D	A	B	C
$D = 0$	saddle point	center point	center point
$0 < D < D_0$	saddle point	center point	center point
$D = D_0$	center point	degraded saddle point	degraded saddle point

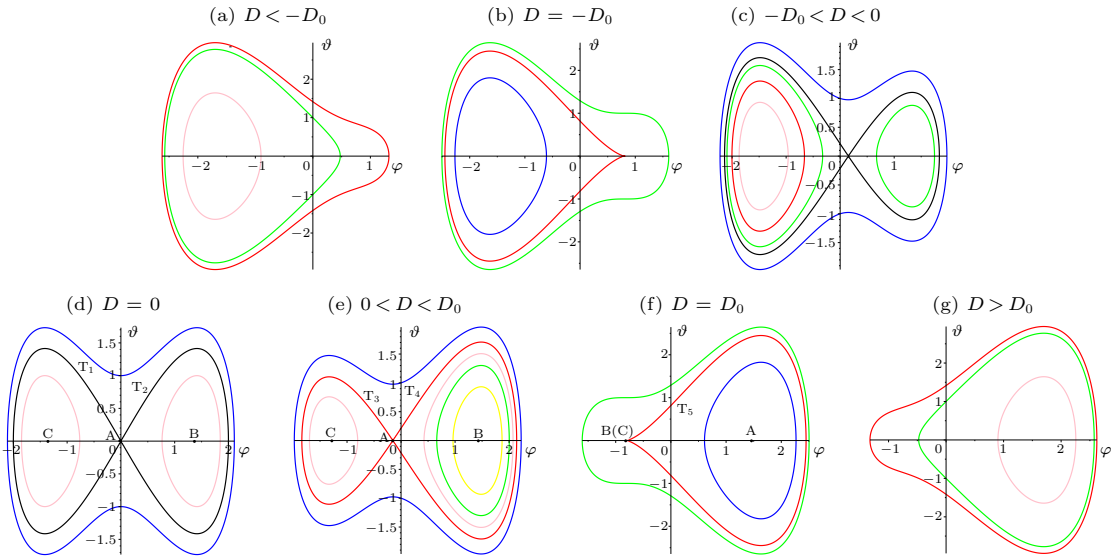


Fig. 2. Phase portraits of system (5) with $b=1$, $k=1$, $a=3$, $\alpha=\frac{1}{2}$, $v=4$: (a) $c=1.5$, (b) $c=\frac{4}{3}\sqrt{\frac{2}{3}}$, (c) $c=0.3$, (d) $c=0$, (e) $c=-0.3$, (f) $c=-\frac{4}{3}\sqrt{\frac{2}{3}}$, (g) $c=-1.5$.

2.3. Analysis for $MN<0$

For $D=0$ and $M>0$, $N<0$ or $M<0$, $N>0$, the phase portraits are plotted in Fig. 3.

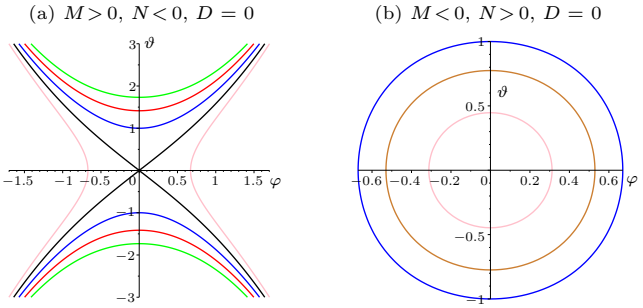


Fig. 3. Phase portraits of system (5) with $b=-1$, $k=1$, $a=3$, $\alpha=1/2$, $v=-4$.

The relevant discussion has been carried out in Ref. [31] and is not be described here.

3. Exact solutions

For a particular ρ, it is well known that $H=\rho$ maps to a level curve of system (5) that determines a solution of Eq. (1). According to the phase portraits, we aim to build parametric representations of exact solutions of Eq. (1), which are not mentioned in Ref. [31].

Firstly, the first equation of system (5) is inserted into Eq. (7), which yields

$$\frac{\mathrm{d}\varphi}{\sqrt{\psi(\varphi)}}=\mathrm{d}\eta, \tag{12}$$

where $\psi(\varphi)=\frac{M}{2}\varphi^4-N\varphi+2D\varphi+2\rho$. For different values of D, various types of solutions are generated after integrating Eq. (12).

3.1. Solutions for $M>0$ and $N>0$

Family I Periodic solutions.

Theorem 1 See orbit L_{10} from Fig. 1(e) corresponding to individual $\rho_2<\rho<\rho_3$. Periodic solution of Eq. (1) is enumerated as

$$u_1=\frac{\varphi_2(\varphi_1-\varphi_3)+\varphi_1(\varphi_3-\varphi_2)\mathrm{sn}^2(E_1,h)}{\varphi_1-\varphi_3+(\varphi_3-\varphi_2)\mathrm{sn}^2(E_1,h)}, \tag{13}$$

where sn denotes the Jacobi elliptic sine function, $E_i=\frac{\sqrt{M(\varphi_4-\varphi_2)(\varphi_3-\varphi_1)}}{2\sqrt{2}}(\eta-\eta_i)$, $h=\sqrt{\frac{(\varphi_3-\varphi_2)(\varphi_4-\varphi_1)}{(\varphi_4-\varphi_2)(\varphi_3-\varphi_1)}}$, $\eta=kx-vt^\alpha$, and η_1 is a constant.

Proof When $\rho_2<\rho<\rho_3$ in Fig. 1(e), the orbits in pink cut the φ axis in four points. For periodic orbit L_{10}, we have

$$\sqrt{\frac{M}{2}}(\eta-\eta_1)=\int_{\varphi_2}^{\varphi}\frac{\mathrm{d}\omega}{\sqrt{(\omega-\varphi_1)(\omega-\varphi_2)(\varphi_3-\omega)(\varphi_4-\omega)}},\quad \varphi_1<\varphi_2<\varphi<\varphi_3<\varphi_4. \tag{14}$$

Periodic solution (13) can be solved from Eq. (14)

Family II Soliton solutions.

Theorem 2 See orbit L_8 from Fig. 1(e). When $\rho=\rho_1$, we calculate a soliton solution of Eq. (1), as shown in Fig. 4,

$$u_2=\varphi_7+\frac{2N-6M\varphi_7^2}{2M\varphi_7+\sqrt{2M(N-M\varphi_7^2)}\cosh\left(\sqrt{3M\varphi_7^2-N}(\eta-\eta_2)\right)}, \tag{15}$$

where $\varphi_5=\frac{-M\varphi_7-\sqrt{2M(N-M\varphi_7^2)}}{M}$, $\varphi_6=\frac{-M\varphi_7+\sqrt{2M(N-M\varphi_7^2)}}{M}$, $\eta=kx-vt^\alpha$, and η_2 is a constant.

Proof This refers to the orbit L_8 in Fig. 1(e). The φ axis is intersected in two points and the point B is double. Therefore, by considering $\{(\varphi,\vartheta)|\vartheta^2=\psi(\varphi),\varphi_5<\varphi_6<\varphi<\varphi_7\}$,

$\psi(\varphi)$ can be rewritten as

$$\psi(\varphi)=\frac{M}{2}(\varphi_7-\varphi)^2(\varphi-\varphi_5)(\varphi-\varphi_6). \tag{16}$$

Equation (12) becomes

$$\sqrt{\frac{M}{2}}(\eta-\eta_2)=\int_{\varphi_6}^{\varphi}\frac{\mathrm{d}\omega}{\sqrt{(\omega-\varphi_5)(\omega-\varphi_6)(\varphi_7-\omega)^2}}. \tag{17}$$

Parametric representation of soliton solution (15) is successfully possessed.

Family Ⅲ Breaking wave solutions.

Theorem 3 (1) See Fig. 1(d).

(i) When $\rho=\rho_2$, Eq. (1) contains two breaking wave solutions, see Fig. 5.

$$u_3=\sqrt{\frac{2N}{M}}\sec[\sqrt{N}(\eta-\eta_3)], \tag{18}$$

$$u_4=\sqrt{\frac{2N}{M}}\csc[\sqrt{N}(\eta-\eta_4)], \tag{19}$$

where $\eta=kx-vt^{\alpha}$, and η_3, η_4 are constants.

(ii) When $\rho_2<\rho<\rho_1$, breaking wave solutions are revealed,

$$u_5=\sqrt{\frac{\varphi_{13}^2-\varphi_{12}^2\mathrm{sn}^2(F_5,m)}{1-\mathrm{sn}^2(F_5,m)}}, \tag{20}$$

$$u_6=\frac{\varphi_{13}}{\mathrm{sn}(F_6,m)}, \tag{21}$$

where $F_i=\varphi_{13}\sqrt{\frac{M}{2}}(\eta-\eta_i)$, $m=\dfrac{\varphi_{12}}{\varphi_{13}}$, $\sqrt{\frac{N}{M}}<\varphi_{13}=-\varphi_{10}<\sqrt{\frac{2N}{M}}$, $\varphi_{12}=-\varphi_{11}=\sqrt{\frac{2N}{M}-\varphi_{13}^2}$, $\eta=kx-vt^{\alpha}$, and η_5, η_6 are constants.

(2) See Fig. 1(e).

(i) When $\rho=\rho_2$, Eq. (1) has solutions

$$u_{7,8}=\varphi_{15}-\frac{2\sigma}{\tau\pm\sqrt{\lambda}\cos\left(\dfrac{\sigma M}{2}(\eta-\eta_7)\right)}, \tag{22}$$

where $\sigma=\frac{-4N+3\varphi_7(M\varphi_7+\sqrt{M(4N-3M\varphi_7^2)})}{M}$, $\tau=-2\varphi_7+\frac{2\sqrt{M(4N-3M\varphi_7^2)}}{M}$, $\lambda=\frac{4\varphi_7(M\varphi_7+\sqrt{M(4N-3M\varphi_7^2)})}{M}$, $\eta=kx-vt^{\alpha}$, and η_7 is a constant.

(ii) When $\rho_2<\rho<\rho_3$, breaking wave solutions are

$$u_9=\frac{\varphi_4(\varphi_3-\varphi_1)-\varphi_3(\varphi_4-\varphi_1)\mathrm{sn}^2(E_8,h)}{\varphi_3-\varphi_1-(\varphi_4-\varphi_1)\mathrm{sn}^2(E_8,h)}, \tag{23}$$

$$u_{10}=\frac{\varphi_1(\varphi_2-\varphi_4)+\varphi_2(\varphi_4-\varphi_1)\mathrm{sn}^2(E_9,h)}{\varphi_2-\varphi_4+(\varphi_4-\varphi_1)\mathrm{sn}^2(E_9,h)}, \tag{24}$$

where $\eta=kx-vt^{\alpha}$, and η_8, η_9 are constants.

(iii) When $\rho=\rho_3$, singular solution is summarized,

$$u_{11}=\varphi_7+\frac{2N-6M\varphi_7^2}{2M\varphi_7-\sqrt{2M(N-M\varphi_7^2)\cosh\left(\sqrt{3M\varphi_7^2-N}(\eta-\eta_{10})\right)}}, \tag{25}$$

where $\eta=kx-vt^{\alpha}$ and η_{10} is a constant.

(3) See Fig. 1(f).

(i) When $\rho=\rho_2$, Eq. (1) provides singular solutions, as shown in Fig. 6,

$$u_{12}=\sqrt{\frac{3N}{M}}\frac{(2N(\eta-\eta_{11})^2+9)}{(6N(\eta-\eta_{11})^2-9)}, \tag{26}$$

$$u_{13,14}=\frac{18\sqrt{2}\pm N\sqrt{3N}(\eta-\eta_{12})^3}{\pm3\sqrt{M}(\eta-\eta_{12})(N(\eta-\eta_{12})^2-6)}, \tag{27}$$

where $\eta=kx-vt^{\alpha}$, and η_{11}, η_{12} are constants.

Proof (1) (i) From the orbits L_6, L_7 in black, we perceive $\{(\varphi,\vartheta)\big|\vartheta^2=\psi(\varphi),\varphi_8<0<\varphi_9<\varphi\}$, $\{(\varphi,\vartheta)\big|\vartheta^2=\psi(\varphi),\varphi<\varphi_8<0<\varphi_9\}$, and integrate Eq. (12) respectively, which gives rise to

$$\sqrt{\frac{M}{2}}(\eta-\eta_3)=\int_{\varphi_9}^{\varphi}\frac{\mathrm{d}\omega}{\sqrt{(\omega-\varphi_8)(\omega-\varphi_9)\omega^2}}, \tag{28}$$

$$\sqrt{\frac{M}{2}}(\eta-\eta_4)=\int_{\varphi}^{+\infty}\frac{\mathrm{d}\omega}{\sqrt{(\varphi_8-\omega)(\varphi_9-\omega)\omega^2}}, \tag{29}$$

where $\varphi_9=-\varphi_8=\sqrt{2N/M}$. Solving Eqs. (28) and (29), we derive solutions (18) and (19).

(ii) Observing open orbits L_4, L_5 drawn in Fig. 1(d), we know that $\{(\varphi,\vartheta)|\vartheta^2=\psi(\varphi),\varphi_3<\varphi_4<0<\varphi_5<\varphi_6<\varphi\}$ and $\{(\varphi,\vartheta)|\vartheta^2=\psi(\varphi),\varphi<\varphi_3<\varphi_4<0<\varphi_5<\varphi_6\}$, which leads

$$\sqrt{\frac{M}{2}}(\eta-\eta_6)=\int_{\varphi_6}^{\varphi}\frac{\mathrm{d}\omega}{\sqrt{(\omega-\varphi_3)(\omega-\varphi_4)(\omega-\varphi_5)(\omega-\varphi_6)}}, \tag{30}$$

$$\sqrt{\frac{M}{2}}(\eta-\eta_7)=\int_{\varphi}^{+\infty}\frac{\mathrm{d}\omega}{\sqrt{(\varphi_3-\omega)(\varphi_4-\omega)(\varphi_5-\omega)(\varphi_6-\omega)}}. \tag{31}$$

Likewise, solutions (20) and (21) are given.

(2) (i) Focus on L_{13}, L_{14} in black in Fig. 1(e). Equivalently, Eq. (12) is individually transformed into

$$\sqrt{\frac{M}{2}}(\eta-\eta_7)=\int_{\varphi_{16}}^{\varphi}\frac{\mathrm{d}\omega}{\sqrt{(\omega-\varphi_{14})(\omega-\varphi_{16})(\omega-\varphi_{15})^2}},\quad \varphi>\varphi_{16}>\varphi_{15}>\varphi_{14}, \tag{32}$$

$$\sqrt{\frac{M}{2}}(\eta-\eta_7)=\int_{\varphi_{14}}^{\varphi}\frac{\mathrm{d}\omega}{\sqrt{(\varphi_{14}-\omega)(\varphi_{16}-\omega)(\varphi_{15}-\omega)^2}},\quad \varphi_{16}>\varphi_{15}>\varphi_{14}>\varphi, \tag{33}$$

where $\varphi_{15}=-\frac{\varphi_9}{2}+\sqrt{\frac{N}{M}-\frac{3\varphi_9^2}{4}}$. Solution (22) is proved by solving Eqs. (32) and (33).

(ii) At this point, the periodic solution corresponding to L_{10} has been established before, and we now focus on L_{11}, L_{12}.

Via utilizing $\{(\varphi,\vartheta)|\vartheta^2=\psi(\varphi),\varphi_1<\varphi_2<\varphi_3<\varphi_4<\varphi\}$ and $\{(\varphi,\vartheta)\big|\vartheta^2=\psi(\varphi),\varphi<\varphi_1<\varphi_2<\varphi_3<\varphi_4\}$, Eq. (12) is severally converted to

$$\sqrt{\frac{M}{2}}(\eta-\eta_8)=\int_{\varphi_4}^{\varphi}\frac{\mathrm{d}\omega}{\sqrt{(\omega-\varphi_1)(\omega-\varphi_2)(\omega-\varphi_3)(\omega-\varphi_4)}}, \tag{34}$$

$$\sqrt{\frac{M}{2}}(\eta-\eta_9)=\int_{\varphi}^{\varphi_1}\frac{\mathrm{d}\omega}{\sqrt{(\varphi_1-\omega)(\varphi_2-\omega)(\varphi_3-\omega)(\varphi_4-\omega)}}. \tag{35}$$

Thus, we exam the solutions (23) and (24).

(iii) See orbit in red on the left of saddle point C, while we have searched the other one in red. Here $\psi(\varphi)$ satisfies

$$\psi(\varphi)=\frac{M}{2}(\varphi_5-\varphi)(\varphi_6-\varphi)(\varphi_7-\varphi)^2,\quad \varphi<\varphi_5<\varphi_6<\varphi_7. \tag{36}$$

Putting Eq. (36) into Eq. (12) and integrating, we prove the existence of solution (25).

(3) (i) The expressions of $\psi(\varphi)$ determined by L_{15}, L_{16} in red are individually

$$\psi(\varphi)=\frac{M}{2}(\varphi-\varphi_{17})(\varphi-\varphi_{18})^3,\quad \varphi_{17}<\varphi_{18}<\varphi, \tag{37}$$

$$\psi(\varphi)=\frac{M}{2}(\varphi_{17}-\varphi)(\varphi_{18}-\varphi)^3,\quad \varphi<\varphi_{17}<\varphi_{18}, \tag{38}$$

where $\varphi_{18}=\sqrt{\frac{N}{3M}}$, $\varphi_{17}=-\sqrt{\frac{3N}{M}}$. Equation (12) becomes

$$\sqrt{\frac{M}{2}}(\eta-\eta_{11})=\int_{\varphi}^{+\infty}\frac{\mathrm{d}\omega}{\sqrt{(\omega-\varphi_{17})(\omega-\varphi_{18})^3}}, \tag{39}$$

$$\sqrt{\frac{M}{2}}(\eta-\eta_{12})=\int_{\varphi_{17}}^{\varphi}\frac{\mathrm{d}\omega}{\sqrt{(\varphi_{17}-\omega)(\varphi_{18}-\omega)^3}}. \tag{40}$$

Solving them, we obtain solutions (26) and (27).

Remark The parametric expressions of the kink (or anti-kink) and periodic solutions in Fig. 1(e) have been listed in Ref. [31], we do not repeat the discussion here.

3.2. Solutions for $M<0$ and $N<0$

Here, we consider the homoclinic orbits as examples to construct all relevant exact parametric expressions of soliton solutions.

Theorem 4 (1) See Fig. 2(d). When $\rho=\rho_2$, two soliton solutions are yielded,

$$u_{15,16}=\pm\sqrt{\frac{2N}{M}}\operatorname{sech}\sqrt{-N}. \tag{41}$$

(2) See Fig. 2(e). When $\rho=\rho_2$, Eq. (1) produces two soliton solutions

$$u_{17}=\varphi_{21}-\frac{2\chi}{(\varphi_{23}-\varphi_{22})\cosh\left(\sqrt{-\frac{M}{2}}\chi(\eta-\eta_{15})\right)-2\varphi_{21}+\varphi_{22}+\varphi_{23}}, \tag{42}$$

$$u_{18}=\varphi_{21}+\frac{2\chi}{(\varphi_{23}-\varphi_{22})\cosh\left(\sqrt{-\frac{M}{2}}\chi(\eta-\eta_{16})\right)+2\varphi_{21}-\varphi_{22}-\varphi_{23}}, \tag{43}$$

where $\chi=(\varphi_{23}-\varphi_{21})(\varphi_{21}-\varphi_{22})$, $\eta=kx-vt^\alpha$, and η_{15}, η_{16} are constants.

(3) See Fig. 2(f). When $\rho=\rho_1$, soliton solution of Eq. (1) is found, see Fig. 7.

$$u_{19}=\sqrt{\frac{N}{3M}}\frac{9bk^3-2\alpha v(\eta-\eta_{17})^2}{3bk^3+2\alpha v(\eta-\eta_{17})^2}, \tag{44}$$

where $\eta=kx-vt^\alpha$ and η_{17} is constant.

Proof (1) We observe that φ-axis is intersected with T_1, T_2 in three points. Thereby, we have

$$\sqrt{\frac{N}{M}}(\eta-\eta_{13})=\int_{\varphi_{20}}^{\varphi}\frac{\mathrm{d}\omega}{-\omega\sqrt{(\varphi_{19}-\omega)(\omega-\varphi_{20})}},\quad \varphi_{20}<\varphi<0<\varphi_{19}, \tag{45}$$

$$\sqrt{\frac{N}{M}}(\eta-\eta_{14})=\int_{\varphi}^{\varphi_{19}}\frac{\mathrm{d}\omega}{\omega\sqrt{(\varphi_{19}-\omega)(\omega-\varphi_{20})}},\quad \varphi_{20}<0<\varphi<\varphi_{19}, \tag{46}$$

where $\varphi_{19}=-\varphi_{20}=\sqrt{2N/M}$, $\eta=kx-vt^\alpha$, and η_{13}, η_{14} are constants. By solving Eqs. (45) and (46), soliton solution (41) is adapted.

(2) For the left orbit T_3, Eq. (12) becomes

$$\sqrt{\frac{N}{M}}(\eta-\eta_{15})=\int_{\varphi_{22}}^{\varphi}\frac{\mathrm{d}\omega}{\sqrt{(\varphi_{23}-\omega)(\omega-\varphi_{22})(\varphi_{21}-\omega)^2}},\quad \varphi_{23}>\varphi_{21}>\varphi>\varphi_{22}. \tag{47}$$

Similarly, for the right orbit T_4, we get

$$\sqrt{\frac{N}{M}}(\eta-\eta_{16})=\int_{\varphi}^{\varphi_{23}}\frac{\mathrm{d}\omega}{\sqrt{(\varphi_{23}-\omega)(\omega-\varphi_{22})(\omega-\varphi_{21})^2}},\quad \varphi_{23}>\varphi>\varphi_{21}>\varphi_{22}. \tag{48}$$

By integrating Eqs. (47) and (48), separately, solutions (42) and (43) are certificated.

(3) The homoclinic orbit T_5 in red is denoted as

$$\psi(\varphi)=\frac{M}{2}(\varphi_{25}-\varphi)(\varphi-\varphi_{24})^3,$$

$$\varphi_{24} < \varphi < \varphi_{25}. \tag{49}$$

Inserting Eq. (49) into Eq. (12) and integrating along T_5, we verify soliton solution (44).

4. Graphic representation

This section pursuits to provide relevant graphs of some solutions in Figs. 4–7.

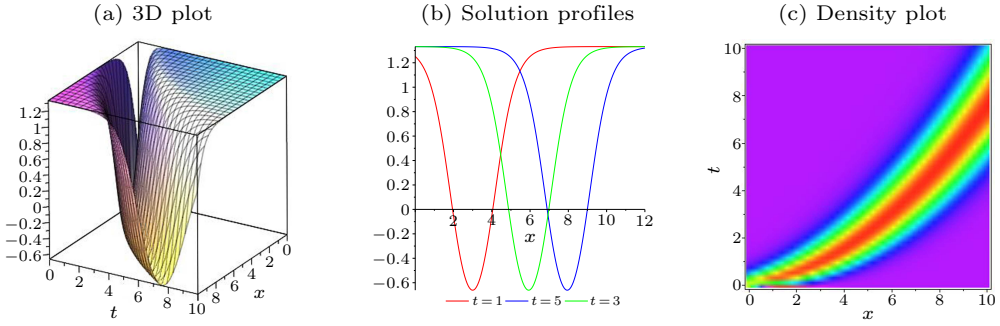


Fig. 4. Dark soliton solution (15) with $\eta_2 = -1$.

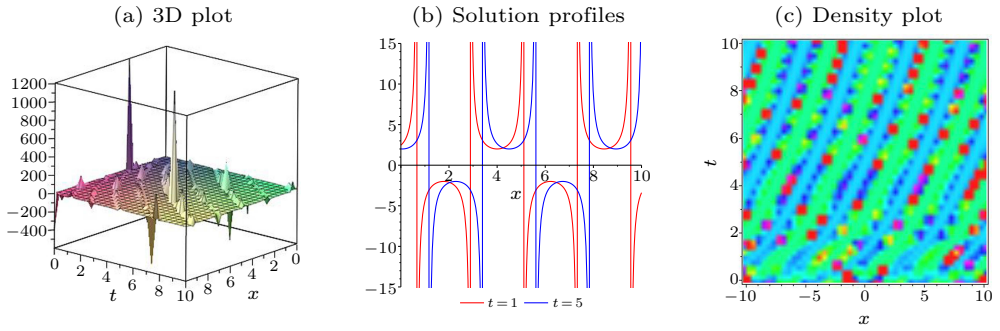


Fig. 5. Singular solution (18) with $\eta_3 = 0$.

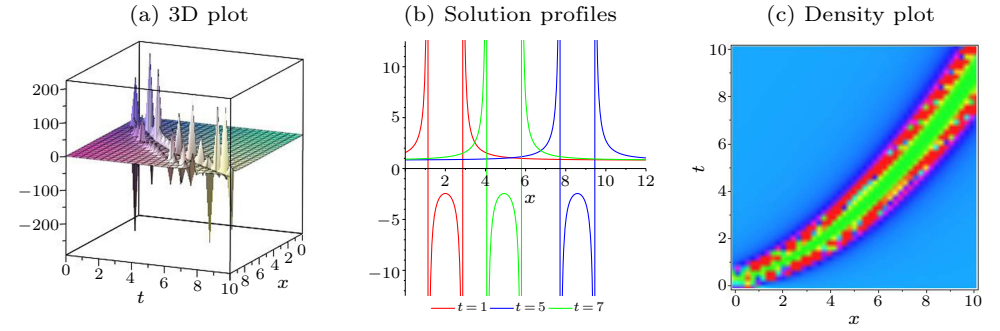


Fig. 6. Singular solution (26) with $\eta_{11} = -2$.

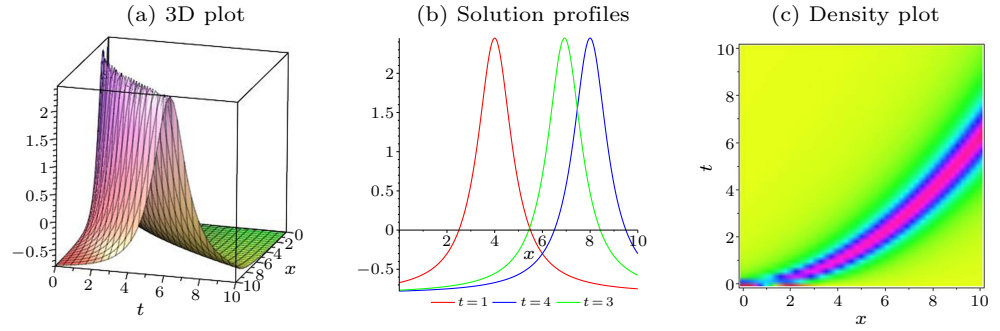


Fig. 7. Bright soliton solution (44).

For Figs. 4–6, choosing appropriate integration constants η_i and $\alpha = 0.5$, $v = 4$, $a = 3$, $b = -1$, $k = 1$, which implies $M = 1$, $N = 2$, we exhibit graphically dark soliton solution u_2, periodic-singular solution u_3 and singular solution u_{12} with the corresponding 3D, density plots and solution profiles, separately. Figure 7 records the behavior of dark solution u_{19} by selecting parameters $\alpha = 0.5$, $\eta_{17} = -2$, $v = 4$, $a = 3$, $b = 1$, $k = 1$, which indicates $M = -1$ and $N = -2$.

5. Conclusion

This work is dedicated to research of exact solutions of the time-fractional modified KdV equation via bifurcation analysis. According to the different orbits of the phase portraits drawn with suitable parameters, the relevant qualitative analysis is concluded. Then, exact solutions of Eq. (1) matching to different types of orbits are constructed successively. Finally, we perform some solutions via presenting solution profiles, 3D and density plots with suitable parametric values.

Acknowledgements

Project supported by the Natural Science Foundation of Shandong Province (Grant No. ZR2021MA084), the Natural Science Foundation of Liaocheng University (Grant No. 318012025), and Discipline with Strong Characteristics of Liaocheng University – Intelligent Science and Technology (Grant No. 319462208).

References

[1] Hirota R 1972 *J. Phys. Soc. Jpn.* **33** 1456
[2] Li L, Duan C N and Yu F J 2019 *Phys. Lett. A* **383** 1578
[3] He J H 2000 *Int. J. Non-Linear Mech.* **35** 37
[4] Elbrolosy M E and Elmandouh A A 2020 *Eur. Phys. J. Plus* **135** 533
[5] Li J B and Chen G R 2005 *Int. J. Bifur. Chaos* **15** 3973
[6] Zhu W J, Xia Y H, Zhang B and Bai Y Zh 2019 *Int. J. Bifur. Chaos* **29** 1950041
[7] Matveev V B and Salle M A 1991 *Darboux Transformations and Solitons* (Berlin: Springer)
[8] Wang M, Tian B and Zhou T Y 2021 *Chaos Solitons Fractals* **152** 111411
[9] Guan X, Liu W J, Zhou Q and Biswas A 2019 *Nonlinear Dyn.* **98** 1491
[10] Kaplan M, Bekir A and Akbulut A 2016 *Nonlinear Dyn.* **85** 2843
[11] Gurefe Y 2020 *Revista Mexicana de Física* **66** 771
[12] Bulut H, Pandir Y and Demiray S T 2014 *Int. J. Model. Optim.* **4** 315
[13] Ma W X 2019 *J. Math. Anal. Appl.* **471** 796
[14] Gkogkou A, Prinari B, Feng B F and Trubatch A D 2022 *Stud. Appl. Math.* **148** 918
[15] Kumar S, Kumar D and Kumar A 2021 *Chaos Solitons Fractals* **142** 110507
[16] Ma W X 2023 *Part. Differ. Equ. Appl. Math.* **7** 100515
[17] Ma W X 2023 *Rep. Math. Phys.* **92** 19
[18] Ma W X 2023 *Int. J. Geometric Methods Mod. Phys.* **20** 2350098
[19] Ma W X 2023 *Appl. Math. Lett.* **145** 108775
[20] Sahoo S and Ray S S 2016 *Physica A* **448** 265
[21] Zafar A 2019 *Nonlinear Eng.* **8** 728
[22] Bhrawy A H, Doha E H, Ezz-Eldien S S and Abdelkawy M A 2015 *Comput. Model. Eng. Sci.* **104** 185
[23] Li C, Kumar A, Kumar S and Yang X J 2016 *Nonlinear Sci. Appl.* **9** 5463
[24] Arshad M S and Iqbal J 2019 *Sci. Inquiry Rev.* **3** 47
[25] Akbulut A and Kaplan M 2018 *Comput. Math. Appl.* **75** 876
[26] Wang G and Xu T 2013 *Boundary Value Problems* **2013** 1
[27] Wen Z 2020 *Appl. Math. Comput.* **366** 124735
[28] Song Y J, Yang B and Wang Z G 2023 *Phys. Lett. A* **461** 128647
[29] Alhamud M, Elbrolosy M and Elmandouh A 2022 *Fractal and Fractional* **7** 16
[30] Yang S 2022 *Scholars J. Phys. Math. Stat.* **7** 109
[31] Liang J L, Tang L K, Xia Y H and Zhang Y 2020 *Int. J. Bifur. Chaos* **30** 2050004
[32] Atangana A, Baleanu D and Alsaedi A 2015 *Open Math.* **13** 889